




 Cite this: *RSC Adv.*, 2019, 9, 8002

# Sulfonyl-bridged (copper-immobilized nickel ferrite) with activated montmorillonite, [(NiFe<sub>2</sub>O<sub>4</sub>@Cu)SO<sub>2</sub>(MMT)]: a new class of magnetically separable clay nanocomposite systems towards Hantzsch synthesis of coumarin-based 1,4-dihydropyridines†

 Behzad Zeynizadeh  and Soleiman Rahmani \*

In this study, the synthesis of a new class of magnetic clay-based nanocomposites by bridging of sulfonyl groups between copper-immobilized nickel ferrite (NiFe<sub>2</sub>O<sub>4</sub>@Cu) and activated montmorillonite is described. Synthesis of the clay nanocatalyst was carried out *via* the activation of montmorillonite by ClSO<sub>3</sub>H to afford sulfonated montmorillonite. The modified montmorillonite was then reacted with copper-layered nickel ferrite to afford the magnetic clay nanocomposite [(NiFe<sub>2</sub>O<sub>4</sub>@Cu)SO<sub>2</sub>(MMT)]. Next, the characterization of porous materials was carried out using scanning electron microscopy, energy-dispersive X-ray spectroscopy, X-ray diffraction, Fourier transform infrared spectroscopy, Brunauer–Emmett–Teller and vibrating sample magnetometer analyses. The obtained results showed that the clay nanocomposite containing a sulfonyl-bridge has a large surface area and magnetic properties *versus* the prepared one without the sulfonyl groups as (NiFe<sub>2</sub>O<sub>4</sub>@Cu)(MMT). The nanostructured clay had excellent catalytic activity towards the Hantzsch synthesis of coumarin-based 1,4-dihydropyridines *via* one-pot and three-component condensation of 4-hydroxycoumarin, aromatic aldehydes and ammonia. All reactions were carried out in water as a green and economic green solvent within 10–45 min to affords 1,4-DHPs in high to excellent yields. Reusability of the clay nanocomposite was investigated for six consecutive cycles without significant loss of catalytic activity. Based on this study, therefore, sulfonated montmorillonite could be considered an excellent support for the immobilization of magnetic materials.

 Received 8th January 2019  
 Accepted 1st March 2019

DOI: 10.1039/c9ra00177h

[rsc.li/rsc-advances](http://rsc.li/rsc-advances)

## 1. Introduction

Nowadays, the immobilization of homogeneous catalysts on the surface of solid supports giving heterogeneous and more stable catalyst systems has gained considerable interest from academic and industrial points of view.<sup>1–4</sup> Accordingly, magnetic spinel ferrites (MFe<sub>2</sub>O<sub>4</sub>; M = Fe, Co, Ni, Mn and Zn) have widespread applications in drug delivery, ferrofluids, pigments, microwave devices, gas sensors and catalysis and have also attracted the attention of scientists.<sup>5–8</sup> Among the spinel ferrites, NiFe<sub>2</sub>O<sub>4</sub> is more desirable. This magnetic material brings several advantages in terms of high saturation magnetization, physical and electrical properties, excellent chemical stability, good mechanical hardness and unique magnetic structure.<sup>9–11</sup> In addition, the combination system of

transition-metal elements with magnetic materials to produce new heterogeneous and magnetically reusable nanocomposite systems has been widely studied and applied towards the promotion of organic transformations.<sup>12</sup> The prepared nanocomposites because of the huge surface area of nanoparticles and formation of numerous acid/base centers dramatically accelerate the rate of reactions. This type of immobilization makes the efficient and easy separation of the catalyst system from the reaction mixture using an external magnetic field. In spite of this, occasionally, after the immobilization of transition metals and because of their high surface energies, the agglomeration of nanoparticles occurs leading to a decrease of effective surface area as well catalytic activity of the prepared nanocatalyst system. In this subject, some strategies have been served to overcome the agglomeration and preserve the original characteristic of nanoparticles. Stabilization of magnetic nanoparticles (MNPs) on porous materials such as silica,<sup>13,14</sup> activated montmorillonite,<sup>15,16</sup> carbon materials,<sup>17–19</sup> zeolites<sup>20</sup> and polymer matrix<sup>21,22</sup> is one of the straightforward methods.

Faculty of Chemistry, Urmia University, Urmia 5756151818, Iran. E-mail: [s.rahmani@urmia.ac.ir](mailto:s.rahmani@urmia.ac.ir)

† Electronic supplementary information (ESI) available. See DOI: 10.1039/c9ra00177h



Montmorillonite (MMT) as aluminosilicate micro/mesoporous material has been widely used in a number of industrial settings and solid supports. This micro/mesoporous material has several advantages in terms of high surface area, swelling, high cation exchange capacity, Brønsted and Lewis acidity, ease of handling, non-corrosiveness and sheet-like structure.<sup>23</sup> Montmorillonite has been also used as a suitable matrix for encapsulation of anisotropic magnetic nanoparticles by their trapping in interlamellar spaces.<sup>15,16,24</sup> The literature review shows that through the acid activation of montmorillonite and exfoliation of adjacent sheets to small segments, the surface properties of montmorillonite such as porosity and specific surface area of the clay mineral could be greatly improved.<sup>25,26</sup> In this context, Xu prepared montmorillonite-based magnetic nanoparticles in water using cetylpyridinium chloride (CPC) as intercalator.<sup>27</sup> Galindo-Gonzalez synthesized magnetite-supported montmorillonite clay particles *via* the electrostatic attraction between  $\text{Fe}_3\text{O}_4$  (positive charge) and MMT layer (negative charge) in collaboration with the negative charge repulsion of MMT layers.<sup>28</sup> Kalantari prepared size-controlled synthesis of  $\text{Fe}_3\text{O}_4$  nanoparticles in the layers of montmorillonite using chemical co-precipitation method.<sup>29</sup> In this area, the synthesis of  $\gamma$ -iron oxide nanoparticles in the layers of montmorillonite has been also reported.<sup>30</sup>

Recently, the application of Cu nanoparticles because of the cheapness, electrical, antifungal, antibacterial properties as well as catalyst for functional group transformations has been considered as one of the most useful transition-metal elements.<sup>31–35</sup> A literature review shows that Cu NPs could be used lonely in the reactions,<sup>35</sup> however, the immobilization form of copper nanoparticles on nickel ferrite ( $\text{NiFe}_2\text{O}_4\text{@Cu}$ )<sup>36</sup> or magnetite ( $\text{Fe}_3\text{O}_4\text{@Cu}$ )<sup>37</sup> was exhibited the better performances.

During the last decades, coumarin-based compounds have been considered as prominent biological active materials and therefore attracted the attention of many scientists. Among the coumarin materials, biscoumarins also showed the significant pharmacological activities such as anti-HIV, anticancer, antifungal, antithrombotic, anti-oxidative, anti-microbial and anti-coagulant<sup>38–41</sup> as well as cytotoxic, enzyme<sup>42,43</sup> and urease inhibitor activities.<sup>44</sup> In this context, numerous reports represented the synthetic importance of biscoumarin materials in the presence of various reagents/catalysts.<sup>45,46</sup> Across the various protocols, using MCRs (multi-components reactions) is one of the straightforward methods for synthesis of this valuable materials. Accordingly, 1,4-dihydropyridines (1,4-DHPs) are also too important materials and received much attention owing to their broad spectrum of biological activities such as anti-cancer, vasodilator, cytotoxic, antidiabetic, antitumor, antimicrobial, antialzheimer and hepatoprotective agents.<sup>47–54</sup> In addition, 1,4-DHPs are also served as L-type  $\text{Ca}^{2+}$  channel blockers to treat hypertension and angina diseases.<sup>55–58</sup> Due course, it would be very interesting that assembling of two mentioned compartments (biscoumarin and 1,4-DHP structures) on a molecule is led to more and new properties attributing to the mentioned therapeutic activities. The literature review shows that using  $\text{Fe}_3\text{O}_4\text{@SiO}_2$ ,<sup>59</sup> guanidinium-based

sulfonic acid,<sup>60</sup> silica gel or acidic alumina/microwave<sup>61</sup> and lactic acid<sup>62</sup> were successfully utilized for synthesis of coumarin-based 1,4-DHPs.

In line with the outlined strategies and continuation of our research program towards synthesis of novel heterogeneous and magnetically nanocomposite systems,<sup>36,37,63–65</sup> herein, we wish to introduce sulfonyl-bridged (copper-immobilized nickel ferrite) with activated montmorillonite,  $[(\text{NiFe}_2\text{O}_4\text{@Cu})\text{SO}_2(\text{MMT})]$ : NFCSM (Fig. 1) representing a new class of magnetically clay nanocomposite systems. The synthesis was carried out with the aims of (i) increasing the catalytic activity of copper-layered nickel ferrite, (ii) preventing the agglomeration of nanoparticles as well as covalently bonding of  $\text{NiFe}_2\text{O}_4\text{@Cu}$  on the surface of the clay mineral, and (iii) improving the stability and shelf-life capability of the nanocatalyst. The examinations resulted that the prepared clay composite system exhibited a perfect catalytic activity towards Hantzsch synthesis of coumarin-based 1,4-dihydropyridines by one-pot and three-component condensation reaction of 4-hydroxycoumarin, aromatic aldehydes and ammonia in water as a green and economic solvent (Scheme 1).

## 2. Experimental

### 2.1. Instruments and reagents

All reagents and substrates were purchased from chemical companies in high purity and they were used without further purification.  $^1\text{H}$ ,  $^{13}\text{C}$  NMR and FT-IR spectra were recorded on Bruker Avance 300 MHz and Thermo Nicolet Nexus 670 spectrometers, respectively. Melting points were measured in open capillary tubes and were uncorrected. TLC was applied for the purity determination of substrates, products and reaction monitoring over silica gel 60 GF254 aluminum sheet. Magnetic properties of the samples were measured by vibrating sample magnetometer (VSM, Meghnatis Daghigh Caviar Co., Iran) under magnetic fields up to 20 kOe. Morphology of the nanoparticles was determined by capturing SEM images using FESEM-TESCAN MIRA3 instrument. The chemical composition

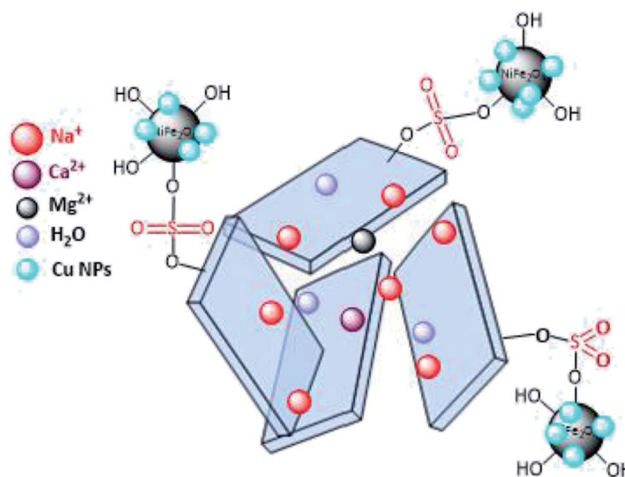
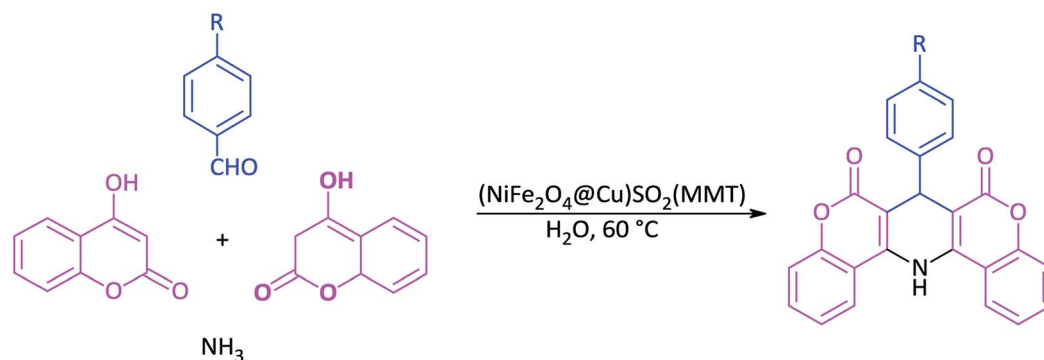


Fig. 1 Magnetic nanoparticles of  $(\text{NiFe}_2\text{O}_4\text{@Cu})\text{SO}_2(\text{MMT})$ .



Scheme 1 Hantzsch synthesis of coumarin-based 1,4-DHPs catalyzed by (NiFe<sub>2</sub>O<sub>4</sub>@Cu)SO<sub>2</sub>(MMT) MNPs.

of nanoparticles was determined by EDX analysis. X-ray diffraction (XRD) measurements were carried out on X'PertPro Panalytical diffractometer in 40 kV and 30 mA with a CuK $\alpha$  radiation ( $\lambda = 1.5418 \text{ \AA}$ ). The specific surface area and total pore volume of the samples were determined using Brunauer–Emmett–Teller method on Belsorp-Max, Japan. The pore size distributions were calculated through the Barrett–Joyner–Halenda method.

## 2.2. Synthesis of NiFe<sub>2</sub>O<sub>4</sub> MNPs

A desired amount of Ni(OAc)<sub>2</sub>·4H<sub>2</sub>O, Fe(NO<sub>3</sub>)<sub>3</sub>·9H<sub>2</sub>O, NaOH and NaCl in a molar ratio of 1 : 2 : 8 : 2, respectively, was grinded in a mortar for 50 min. The reaction was exothermic and accompanied with the release of heat. It is notable that through the grinding of the mixture, the synthesis of NiFe<sub>2</sub>O<sub>4</sub> was initiated. After completion of the reaction, the mixture was then washed several times with deionized water to remove NaCl and other contaminants. The obtained solid material was then dried at 80 °C for 10 h. The resulting product was calcinated at 900 °C for 2 h to obtain magnetically nanoparticles of NiFe<sub>2</sub>O<sub>4</sub>.

## 2.3. Synthesis of NiFe<sub>2</sub>O<sub>4</sub>@Cu MNPs

In a round-bottom flask containing a solution of CuCl<sub>2</sub>·2H<sub>2</sub>O (0.25 g) in deionized water (30 mL), magnetic nanoparticles of NiFe<sub>2</sub>O<sub>4</sub> (1 g) was added. The mixture was stirred for 30 min at room temperature followed with the addition of NaBH<sub>4</sub> (0.11 g in 30 mL H<sub>2</sub>O) within 20 min in drop wise manner (N<sub>2</sub> atmosphere). The mixture was continued to stirring for 2 h. The precipitated nanoparticles of NiFe<sub>2</sub>O<sub>4</sub>@Cu were magnetically separated and then washed with deionized water. Drying under vacuum affords NiFe<sub>2</sub>O<sub>4</sub>@Cu MNPs.<sup>36</sup>

## 2.4. Preparation of homoionic Na<sup>+</sup>-montmorillonite (Na<sup>+</sup>-MMT)

In a beaker (250 mL) containing a solution of NaCl (200 mL, 2 M), montmorillonite K10 (MMT-K10) (5 g) was added and the mixture was stirred vigorously for 78 h at room temperature. After that, mesoporous particles of homoionic Na<sup>+</sup>-montmorillonite were separated by centrifugation. The particles were washed with deionized water followed by drying in an oven at 50 °C for 12 h.<sup>66,67</sup>

## 2.5. Preparation of sulfonated sodium montmorillonite (Na<sup>+</sup>-MMT-SO<sub>3</sub>H)

In a round-bottom flask, a suspension of Na<sup>+</sup>-montmorillonite (2.5 g) in CHCl<sub>3</sub> (5 mL) and in an ice bath (0–5 °C) was prepared. Through a dropping funnel, ClSO<sub>3</sub>H (0.5 g, 9 mmol) was added in a drop wise manner within 30 min. After that, the mixture was stirred for additional 30 min for complete releasing of HCl. The mixture was then filtered and the solid residue was washed with MeOH (20 mL) and dried at room temperature to obtain Na<sup>+</sup>-MMT-SO<sub>3</sub>H as a white powder.

## 2.6. Synthesis of (NiFe<sub>2</sub>O<sub>4</sub>@Cu)SO<sub>2</sub>(MMT) MNPs

An individual suspension of Na<sup>+</sup>-MMT-SO<sub>3</sub>H (3 g) in deionized water (200 mL, pH value of the resulting suspension was adjusted to ~5 by 3 wt% HCl) and NiFe<sub>2</sub>O<sub>4</sub>@Cu (1.5 g) in deionized water (200 mL, pH value of the resulting suspension was adjusted to ~9 by 3 wt% ammonia) was irradiated by ultrasound for 30 min. Two suspensions were combined together followed by stirring for 2 h. The prepared nanocomposite of (NiFe<sub>2</sub>O<sub>4</sub>@Cu)SO<sub>2</sub>(MMT) were separated by magnetic decantation and then washed with EtOH. Drying under vacuum afforded the final nanocomposite in a feeding weight ratio of 2 : 1 for Na<sup>+</sup>-MMT-SO<sub>3</sub>H/NiFe<sub>2</sub>O<sub>4</sub>@Cu, respectively.

## 2.7. Synthesis of (NiFe<sub>2</sub>O<sub>4</sub>@Cu)(MMT) MNPs

An individual suspension of Na<sup>+</sup>-MMT (3 g) in deionized water (200 mL, pH value of the resulting suspension was adjusted to ~5 by 3 wt% HCl) and NiFe<sub>2</sub>O<sub>4</sub>@Cu (1.5 g) in deionized water (200 mL, pH value of the resulting suspension was adjusted to ~9 by 3 wt% ammonia) was irradiated by ultrasound for 30 min. Two suspensions were combined together followed by stirring for 2 h. The prepared nanocomposite of (NiFe<sub>2</sub>O<sub>4</sub>@Cu)(MMT) were separated by magnetic decantation and then washed with EtOH. Drying under air atmosphere affords (NiFe<sub>2</sub>O<sub>4</sub>@Cu)(MMT) MNPs.

## 2.8. Synthesis of (NiFe<sub>2</sub>O<sub>4</sub>@Cu)(MMT-SO<sub>3</sub>H) MNPs

The prepared (NiFe<sub>2</sub>O<sub>4</sub>@Cu)(MMT) (3 g) was added to a solution of ClSO<sub>3</sub>H (0.5 g, 9 mmol) in CHCl<sub>3</sub> (5 mL) (0–5 °C) within

30 min. After that, the mixture was stirred for 30 min for complete releasing of HCl. The mixture was then filtered and the solid residue was washed with MeOH and dried at room temperature to obtain (NiFe<sub>2</sub>O<sub>4</sub>@Cu)(MMT-SO<sub>3</sub>H) MNPs.

## 2.9. A general procedure for Hantzsch synthesis of coumarin-based 1,4-DHPs catalyzed by (NiFe<sub>2</sub>O<sub>4</sub>@Cu)SO<sub>2</sub>(MMT) MNPs

In a round-bottom flask (15 mL), a mixture of 4-hydroxycoumarin (2 mmol), aromatic aldehyde (1 mmol) and ammonia (2 mmol) in water (2 mL) was prepared. Magnetically nanoparticles of (NiFe<sub>2</sub>O<sub>4</sub>@Cu)SO<sub>2</sub>(MMT) (10 mg) was then added and the resulting mixture was stirred at 60 °C for an appropriate time (Table 6). After completion of the reaction (monitored with by TLC), DMSO (2 mL) was added to the reaction mixture: the catalyst was insoluble in DMSO and easily separated by an external magnetic field. After that, a saturated solution of NaCl was added. In a meanwhile of the addition, 1,4-DHP was precipitated, filtered and washed with *n*-hexane.

## 2.10. Selected spectral data

**2.10.1. 7-Phenyl-7,14-dihydro-6*H*,8*H*-dichromeno[4,3-*b*:3',4'-*e*]pyridine-6,8-dione (4a).** FT-IR (KBr,  $\nu$  cm<sup>-1</sup>): 3435, 3196, 3049, 1659, 1610, 1540, 1406, 1266, 1185, 1108, 1039, 901, 755; <sup>1</sup>H NMR (300 MHz, DMSO-d<sub>6</sub>)  $\delta$  (ppm) 6.30 (s, 1H, CH<sub>benzylic</sub>), 7.01–7.38 (m, 10H, ArH and NH), 7.45–7.55 (m, 2H, ArH), 7.82 (d, 2H, ArH); <sup>13</sup>C NMR (75 MHz, DMSO-d<sub>6</sub>)  $\delta$  (ppm) 36.5, 103.7, 115.9, 120.1, 123.5, 124.5, 125.4, 127, 128.2, 131.5, 142.5, 152.8, 165.3, 168.3.

**2.10.2. 7-(2-Chlorophenyl)-7,14-dihydro-6*H*,8*H*-dichromeno[4,3-*b*:3',4'-*e*]pyridine-6,8-dione (4b).** FTIR (KBr,  $\nu$  cm<sup>-1</sup>): 3418, 3182, 1769, 1604, 1489, 1406, 1188, 1041, 944, 758; <sup>1</sup>H NMR (300 MHz, DMSO)  $\delta$  6.15 (s, 1H, CH<sub>benzylic</sub>), 7.15–7.40 (m, 8H, ArH and NH), 7.40–7.60 (m, 3H, ArH), 7.80 (d, 2H, ArH); <sup>13</sup>C NMR (75 MHz, DMSO)  $\delta$  36.5, 103.2, 115.2, 115.9, 120.3, 123.4, 124.4, 127.4, 130.88, 131.2, 133.1, 140.8, 152.8, 164.3, 164.3, 168.1.

**2.10.3. 7-(4-Chlorophenyl)-7,14-dihydro-6*H*,8*H*-dichromeno[4,3-*b*:3',4'-*e*]pyridine-6,8-dione (4c).** FT-IR (KBr,  $\nu$  cm<sup>-1</sup>): 3183, 3046, 2594, 1611, 1540, 1407, 1186, 1099, 1029, 903, 757; <sup>1</sup>H NMR (300 MHz, DMSO-d<sub>6</sub>)  $\delta$  (ppm) 6.23 (s, 1H, CH<sub>benzylic</sub>), 6.93 (s, 1H, NH), 7.05–7.18 (m, 2H, ArH), 7.18–7.35 (m, 6H, ArH), 7.45–7.60 (m, 2H, ArH), 7.80 (d, 2H, ArH); <sup>13</sup>C NMR (75 MHz, DMSO-d<sub>6</sub>)  $\delta$  (ppm) 36.2, 103.5, 115.9, 120.2, 123.3, 124.5, 128, 128.9, 129.8, 131.4, 166.8.

**2.10.4. 7-(3-Hydroxy-4-methoxyphenyl)-7,14-dihydro-6*H*,8*H*-dichromeno[4,3-*b*:3',4'-*e*]pyridine-6,8-dione (4d).** FT-IR (KBr,  $\nu$  cm<sup>-1</sup>): 3411, 3142, 3047, 2927, 2851, 1661, 1611, 1562, 1510, 1406, 1270, 1098, 1028, 906, 760; <sup>1</sup>H NMR (300 MHz, DMSO-d<sub>6</sub>)  $\delta$  (ppm) 3.68 (s, 3H, OMe), 6.14 (s, 1H, CH<sub>benzylic</sub>), 6.42–6.55 (m, 1H, ArH), 6.55–6.65 (m, 1H, ArH), 6.65–6.75 (m, 1H, ArH), 7.15–7.27 (m, 5H, ArH and NH), 7.41–7.58 (m, 2H, ArH), 7.82 (d, 2H, ArH), 8.60 (bs, 1H, OH); <sup>13</sup>C NMR (75 MHz, DMSO-d<sub>6</sub>)  $\delta$  (ppm) 35.1, 54.1, 104, 112.4, 114.8, 115.8, 117.6, 120.4, 131.3, 135.2, 145.5, 152.9, 165.2, 168.2.

**2.10.5. 7-(4-Hydroxy-3-methoxyphenyl)-7,14-dihydro-6*H*,8*H*-dichromeno[4,3-*b*:3',4'-*e*]pyridine-6,8-dione (4e).** FT-IR (KBr,  $\nu$  cm<sup>-1</sup>): 3410, 3218, 3069, 2931, 1651, 1607, 1514, 1448, 1403, 1277, 1185, 1114, 1034, 760; <sup>1</sup>H NMR (300 MHz, DMSO-d<sub>6</sub>)

$\delta$  (ppm) 3.37 (s, 3H, OMe), 6.17 (s, 1H, CH<sub>benzylic</sub>), 6.45–6.67 (m, 3H, ArH), 7.05–7.33 (m, 5H, ArH and NH), 7.42–7.58 (m, 2H, ArH), 7.81 (d, 2H, ArH), 8.51 (bs, 1H, OH); <sup>13</sup>C NMR (75 MHz, DMSO-d<sub>6</sub>)  $\delta$  (ppm) 35.9, 56.1, 104.2, 112.2, 115.2, 119.7, 120.4, 123.3, 131.2, 133.6, 144.5, 147.4, 152.9, 165, 168.1.

**2.10.6. 7-(3-Methoxyphenyl)-7,14-dihydro-6*H*,8*H*-dichromeno[4,3-*b*:3',4'-*e*]pyridine-6,8-dione (4f).** FT-IR (KBr,  $\nu$  cm<sup>-1</sup>): 3421, 3073, 3066, 1645, 1603, 1523, 1417, 1268, 1205, 1043, 973, 897, 761; <sup>1</sup>H NMR (300 MHz, DMSO-d<sub>6</sub>)  $\delta$  (ppm) 3.72 (s, 3H, OMe), 5.45 (s, 1H, CH<sub>benzylic</sub>), 6.82 (s, 1H, ArH), 7.05–7.35 (m, 7H, ArH and NH), 7.35–7.60 (m, 1H, ArH), 7.83 (bs, 1H, ArH), 8.32 (bs, 3H, ArH); <sup>13</sup>C NMR (75 MHz, DMSO-d<sub>6</sub>)  $\delta$  (ppm) 35.7, 94.1, 103.7, 109.7, 113.7, 119.7, 122.4, 123, 141.9, 144.5, 152.9, 159.5, 165, 168.2.

**2.10.7. 7-(*p*-Tolyl)-7,14-dihydro-6*H*,8*H*-dichromeno[4,3-*b*:3',4'-*e*]pyridine-6,8-dione (4h).** FT-IR (KBr,  $\nu$  cm<sup>-1</sup>): 3433, 2927, 1671, 1613, 1412, 1189, 1039, 763; <sup>1</sup>H NMR (300 MHz, DMSO-d<sub>6</sub>)  $\delta$  (ppm) 2.19 (s, 3H, Me), 6.20 (s, 1H, CH<sub>benzylic</sub>), 6.94 (s, 4H, ArH), 7.18–7.25 (m, 5H, ArH and NH), 7.41–7.55 (m, 2H, ArH), 7.78 (d, 2H, ArH); <sup>13</sup>C NMR (75 MHz, DMSO-d<sub>6</sub>)  $\delta$  (ppm) 22.2, 36.1, 103.9, 120.4, 124.5, 128.7, 131.2, 133.9, 152.9, 165, 168.1.

**2.10.8. 7-(4-Nitrophenyl)-7,14-dihydro-6*H*,8*H*-dichromeno[4,3-*b*:3',4'-*e*]pyridine-6,8-dione (4j).** FT-IR (KBr,  $\nu$  cm<sup>-1</sup>): 3463, 3202, 3067, 2912, 1667, 1608, 1534, 1513, 1339, 1341, 1181, 1109, 1043, 942, 850, 762; <sup>1</sup>H NMR (300 MHz, DMSO-d<sub>6</sub>)  $\delta$  (ppm) 6.33 (s, 1H, CH<sub>benzylic</sub>), 7.15–7.30 (m, 5H, ArH and NH), 7.30–7.40 (m, 2H, ArH), 7.45–7.61 (m, 2H, ArH), 7.75–7.85 (m, 2H, ArH), 8.01–8.13 (m, 2H, ArH); <sup>13</sup>C NMR (75 MHz, DMSO-d<sub>6</sub>)  $\delta$  (ppm) 37.1, 103.2, 116, 120.1, 122.8, 124.2, 125.7, 131.6, 145.7, 151.9, 153, 164.8, 168.4.

**2.10.9. 7-(3-Nitrophenyl)-7,14-dihydro-6*H*,8*H*-dichromeno[4,3-*b*:3',4'-*e*]pyridine-6,8-dione (4k).** FT-IR (KBr,  $\nu$  cm<sup>-1</sup>): 3437, 3213, 3066, 1611, 1530, 1415, 1345, 1183, 1045, 850, 758; <sup>1</sup>H NMR (300 MHz, DMSO-d<sub>6</sub>)  $\delta$  (ppm) 6.34 (s, 1H, CH<sub>benzylic</sub>), 7.21–7.82 (m, 11H, ArH and NH), 7.88 (s, 1H, ArH), 7.97 (s, 1H, ArH); <sup>13</sup>C NMR (75 MHz, DMSO-d<sub>6</sub>)  $\delta$  (ppm) 36.7, 103, 116, 120.1, 123.5, 123.5, 129.8, 131.7, 145.6, 153, 164.8, 168.4.

**2.10.10. 7-(4-Chloro-3-nitrophenyl)-7,14-dihydro-6*H*,8*H*-dichromeno[4,3-*b*:3',4'-*e*]pyridine-6,8-dione (4l).** FT-IR (KBr,  $\nu$  cm<sup>-1</sup>): 3429, 3100, 2900, 1664, 1608, 1537, 1406, 1352, 1188, 1042, 834, 764; <sup>1</sup>H NMR (300 MHz, DMSO-d<sub>6</sub>)  $\delta$  (ppm) 6.29 (s, 1H, CH<sub>benzylic</sub>), 7.15–7.30 (m, 5H, ArH and NH), 7.35–7.45 (m, 1H, ArH), 7.45–7.62 (m, 3H, ArH), 7.68 (s, 1H, ArH), 7.75–7.85 (m, 2H, ArH); <sup>13</sup>C NMR (75 MHz, DMSO-d<sub>6</sub>)  $\delta$  (ppm) 36.4, 102.8, 116, 120.1, 123.5, 124.5, 131.4, 132.8, 144.6, 153, 164.7, 168.4.

## 3. Results and discussion

### 3.1. Synthesis and characterization of (NiFe<sub>2</sub>O<sub>4</sub>@Cu)SO<sub>2</sub>(MMT) MNPs

Synthesis of the magnetic sulfonyl-bridged clay composite, NFCSM, was carried out through a five-step procedure: (i) preparation of NiFe<sub>2</sub>O<sub>4</sub> MNPs *via* a solid state grinding of Ni(OAc)<sub>2</sub>·4H<sub>2</sub>O and Fe(NO<sub>3</sub>)<sub>3</sub>·9H<sub>2</sub>O in the presence of NaOH, (ii) mixing of NiFe<sub>2</sub>O<sub>4</sub> MNPs with an aqueous solution of CuCl<sub>2</sub>·2H<sub>2</sub>O, (iii) reduction of Cu<sup>2+</sup> ions to Cu<sup>0</sup> with NaBH<sub>4</sub> to afford NiFe<sub>2</sub>O<sub>4</sub>@Cu MNPs, (iv) preparation of acid-activated sodium montmorillonite (Na<sup>+</sup>-MMT-SO<sub>3</sub>H) by stirring of

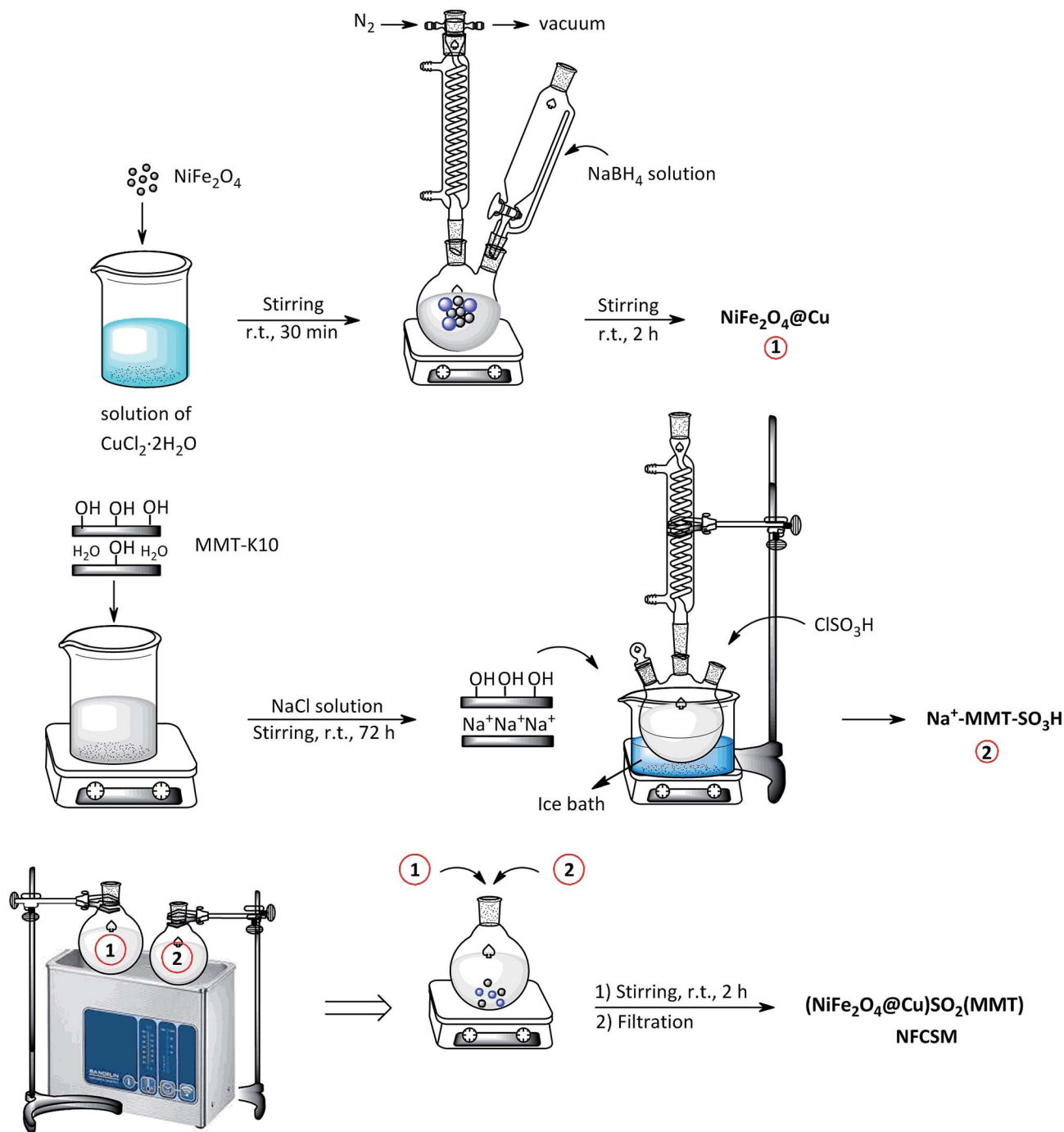


Fig. 2 Preparing of  $(\text{NiFe}_2\text{O}_4 @ \text{Cu})\text{SO}_2(\text{MMT})$  MNPs.

homoionic  $\text{Na}^+$ -exchanged montmorillonite with  $\text{ClSO}_3\text{H}$ , and finally (v) preparation of  $(\text{NiFe}_2\text{O}_4 @ \text{Cu})\text{SO}_2(\text{MMT})$  via the reaction of individual sonicated-suspension of  $\text{NiFe}_2\text{O}_4 @ \text{Cu}$  and  $\text{Na}^+ \text{-MMT-SO}_3\text{H}$  (Fig. 2).

It is notable that in the preparation of sulfonyl-bridged clay composite system (NFCSM), the selection of proper solvent and pH value of the suspensions is crucial. In this context, the examinations resulted that dispersity of  $\text{Na}^+ \text{-MMT}$ ,  $\text{NiFe}_2\text{O}_4 @ \text{Cu}$  and  $\text{Na}^+ \text{-MMT-SO}_3\text{H}$  in  $\text{H}_2\text{O}$  is higher than the other solvents and therefore it was selected as the solvent of choice to carry out the synthetic reaction (Table 1).

It was also reported that the yield and magnetic property of metal oxides could be influenced effectively by pH value.<sup>26</sup> Consequently, we investigated the influence of pH on the yield

Table 1 Dispersity of  $\text{Na}^+ \text{-MMT}$ ,  $\text{NiFe}_2\text{O}_4 @ \text{Cu}$  and  $\text{Na}^+ \text{-MMT-SO}_3\text{H}$  in different solvents

Sample	$\text{H}_2\text{O}$	EtOH 90%	Acetone	DMF	$\text{CHCl}_3$
$\text{Na}^+ \text{-MMT}$	Well	Medium	Well	Weak	Weak
$\text{NiFe}_2\text{O}_4 @ \text{Cu}$	Well	Medium	Weak	Weak	Weak
$\text{Na}^+ \text{-MMT-SO}_3\text{H}$	Well	Well	Well	Weak	Weak

**Table 2** The influence of pH on the yield and magnetic property of  $(\text{NiFe}_2\text{O}_4@\text{Cu})\text{SO}_2(\text{MMT})$  MNPs

pH value of $\text{Na}^+$ -MMT- $\text{SO}_3\text{H}$ (A)	pH value of $\text{NiFe}_2\text{O}_4@\text{Cu}$ (B)	pH value of mixing A + B	Yield of $(\text{NFCSM})^a$ (%)	$M_s$ value of (NFCSM) ( $\text{emu g}^{-1}$ )
3	12	10	90	1.75
5	9	8	95	3.03
6	8	7	87	2.8

$$^a \text{Yield} = [W_{\text{composite}} / (W_{\text{Na}^+\text{-MMT-}\text{SO}_3\text{H}} + W_{\text{NiFe}_2\text{O}_4@\text{Cu}})] \times 100.$$

and magnetic property of sulfonyl-bridged clay composite (NFCSM). The results of this investigation are illustrated in Table 2. The table shows that accessing high magnetic property and yield of NFCSM required pH value of 9 and 5 for suspensions of  $\text{NiFe}_2\text{O}_4@\text{Cu}$  and  $\text{Na}^+$ -MMT- $\text{SO}_3\text{H}$ , respectively. Adjusting of pH values was carried out by adding the proper amounts of HCl or ammonia to the suspensions.

### 3.2. Characterization of the clay-based nanocomposites

**3.2.1. XRD analysis.** Wide-angle XRD spectra of MMT-K10,  $\text{Na}^+$ -MMT,  $\text{Na}^+$ -MMT- $\text{SO}_3\text{H}$ ,  $(\text{NiFe}_2\text{O}_4@\text{Cu})\text{SO}_2(\text{MMT})$ ,  $(\text{NiFe}_2\text{O}_4@\text{Cu})(\text{MMT})$  and  $(\text{NiFe}_2\text{O}_4@\text{Cu})(\text{MMT-}\text{SO}_3\text{H})$  are shown in Fig. 3. In diffractogram of montmorillonite K10 (pattern a) and along with  $hkl$  and two dimensional  $hk$  reflections, a number of sharp peaks attributing to some impurities (quartz, cristobalite and feldspar) is observable. As well, the pattern b shows that during the homoionization of MMT-K10 with NaCl and diffusion of  $\text{Na}^+$  ions into interlamellar spaces of montmorillonite (through ion-exchange ability), the signal-intensity of  $\text{Na}^+$ -MMT was raised.<sup>67</sup> In contrast and in the case of  $\text{Na}^+$ -MMT- $\text{SO}_3\text{H}$  (pattern c), due covalently bonding of sulfonic acid moiety instead of  $\text{Na}^+$  ions, the signal-intensity was downed. According to the standard diffraction pattern of  $\text{NiFe}_2\text{O}_4$  (JCPDS 44-1485), diffractogram of  $(\text{NiFe}_2\text{O}_4@\text{Cu})$  (pattern d) shows that during the immobilization of copper on  $\text{NiFe}_2\text{O}_4$ , the cubic spinel structure of  $\text{NiFe}_2\text{O}_4$  was remained intact. Moreover, comparing the XRD pattern of  $(\text{NiFe}_2\text{O}_4@\text{Cu})$  (pattern d),  $[(\text{NiFe}_2\text{O}_4@\text{Cu})(\text{MMT})]$  (pattern e) and  $[(\text{NiFe}_2\text{O}_4@\text{Cu})\text{SO}_2(\text{MMT})]$  (pattern f) represents that both of the prepared  $[(\text{NiFe}_2\text{O}_4@\text{Cu})(\text{MMT})]$  and  $[(\text{NiFe}_2\text{O}_4@\text{Cu})\text{SO}_2(\text{MMT})]$  include the characteristic peaks of  $\text{NiFe}_2\text{O}_4@\text{Cu}$  MNPs. This is showing that magnetically nanoparticle of  $\text{NiFe}_2\text{O}_4@\text{Cu}$  was highly dispersed on the surface of clay matrix and missed its some crystallinity character.<sup>68,69</sup> Similarly, the same discussion is given for montmorillonite moiety through the grafting of  $\text{NiFe}_2\text{O}_4@\text{Cu}$  MNPs. It is meaning that by combining  $\text{NiFe}_2\text{O}_4@\text{Cu}$  moiety with montmorillonite, no structural change was occurred in the clay matrix. In addition, XRD pattern of  $(\text{NiFe}_2\text{O}_4@\text{Cu})(\text{MMT-}\text{SO}_3\text{H})$  (pattern g) clearly shows the characteristic signals of  $\text{NiFe}_2\text{O}_4@\text{Cu}$  MNPs.

**3.2.2. SEM analysis.** Scanning electron microscopy (SEM) is a useful technique to elucidate the porosity and surface morphology of materials. In this area, SEM images of montmorillonite K10 (Fig. 4a and b) show that the clay mineral is multilayer material with parallel arrays of large flakes. In the

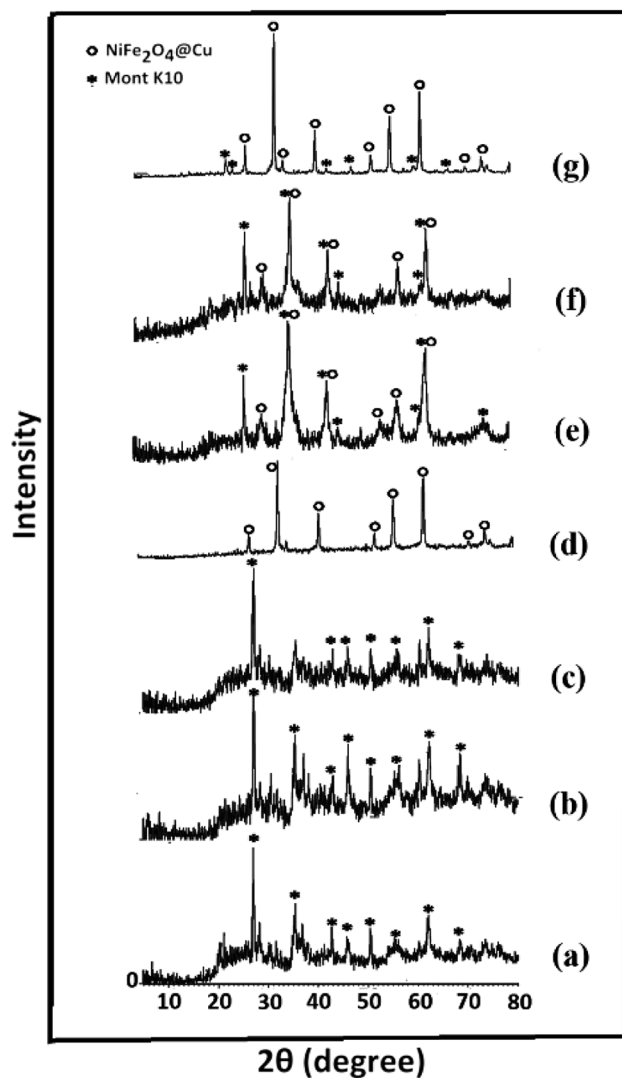


**Fig. 3** Wide-angle XRD patterns of (a) MMT-K10, (b)  $\text{Na}^+$ -MMT, (c)  $\text{Na}^+$ -MMT- $\text{SO}_3\text{H}$ , (d)  $\text{NiFe}_2\text{O}_4@\text{Cu}$ , (e)  $(\text{NiFe}_2\text{O}_4@\text{Cu})\text{SO}_2(\text{MMT})$ , (f)  $(\text{NiFe}_2\text{O}_4@\text{Cu})(\text{MMT})$  and (g)  $(\text{NiFe}_2\text{O}_4@\text{Cu})(\text{MMT-}\text{SO}_3\text{H})$ .

case of  $(\text{NiFe}_2\text{O}_4@\text{Cu})\text{SO}_2(\text{MMT})$ , the SEM images (Fig. 4d–f) represent that after the sulfonation process of montmorillonite K10 and grafting of  $\text{NiFe}_2\text{O}_4@\text{Cu}$  MNPs, large flakes of MMT-K10 were exfoliated to small segments with semi-flat surfaces.<sup>70,71</sup> The images also exhibit that magnetically nanoparticles of  $\text{NiFe}_2\text{O}_4@\text{Cu}$  MNPs with average size of 16 nm were immobilized on the surface of clay matrix. Accordingly, EDX analyses exhibited the presence of Ni, Fe and Cu elements in  $(\text{NiFe}_2\text{O}_4@\text{Cu})\text{SO}_2(\text{MMT})$  (Fig. 4g) as well as the elements of MMT-K10 (Fig. 4c).

**3.2.3.  $\text{N}_2$  adsorption-desorption study.** The  $\text{N}_2$  adsorption-desorption isotherm of  $(\text{NiFe}_2\text{O}_4@\text{Cu})\text{SO}_2(\text{MMT})$ ,  $(\text{NiFe}_2\text{O}_4@\text{Cu})(\text{MMT})$  and  $(\text{NiFe}_2\text{O}_4@\text{Cu})(\text{MMT-}\text{SO}_3\text{H})$  are illustrated in Fig. 5. Investigation of the results shows that the shape of isotherms in  $(\text{NiFe}_2\text{O}_4@\text{Cu})\text{SO}_2(\text{MMT})$  and  $(\text{NiFe}_2\text{O}_4@\text{Cu})(\text{MMT-}\text{SO}_3\text{H})$  MNPs are similar and according to BDDT classification is closer to isotherm of Langmuir (isotherm type I). This type of isotherms is a characteristic of mesoporous solid

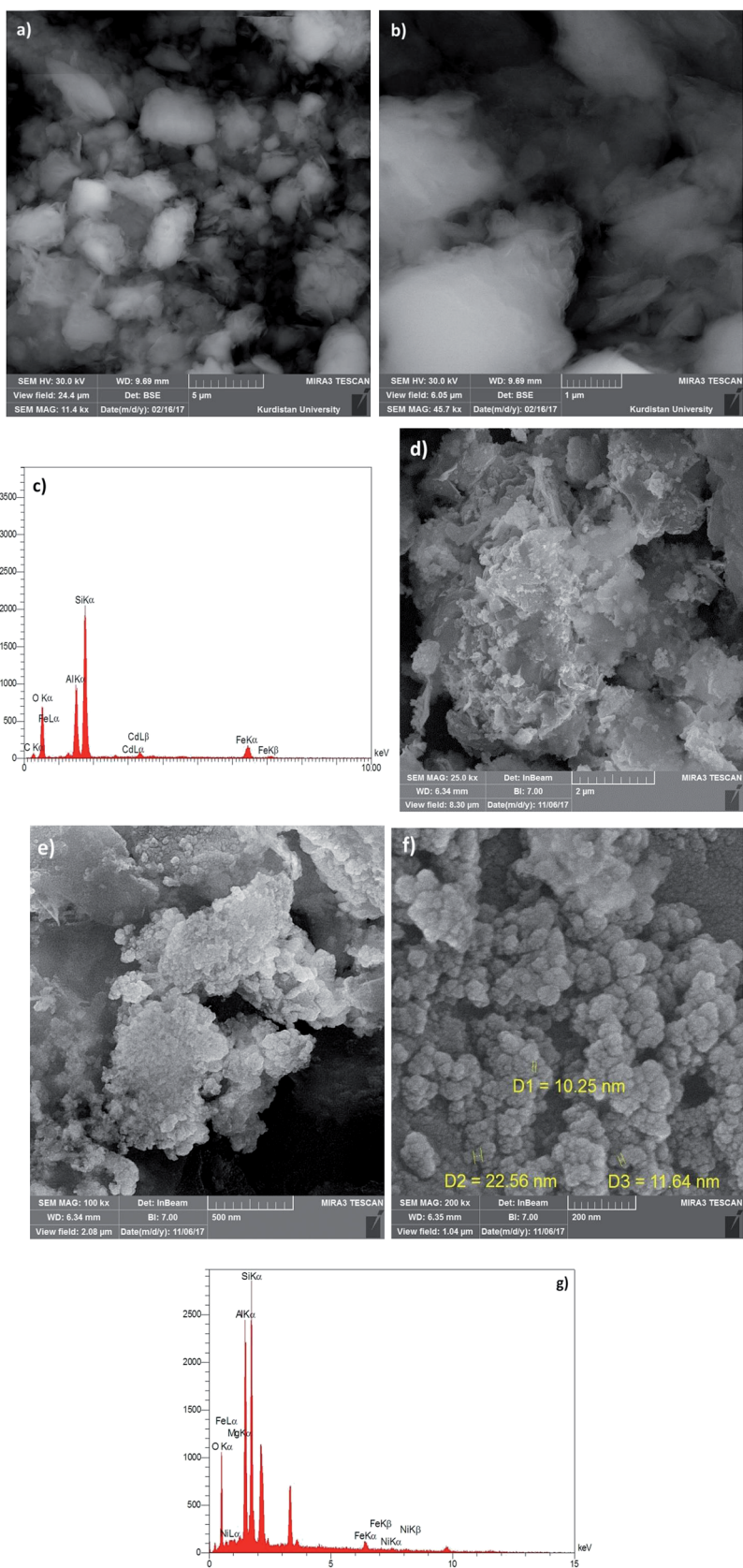


Fig. 4 SEM images and EDX spectra of MMT-K10 (a–c) and (NiFe<sub>2</sub>O<sub>4</sub>@Cu)SO<sub>2</sub>(MMT) (d–g).

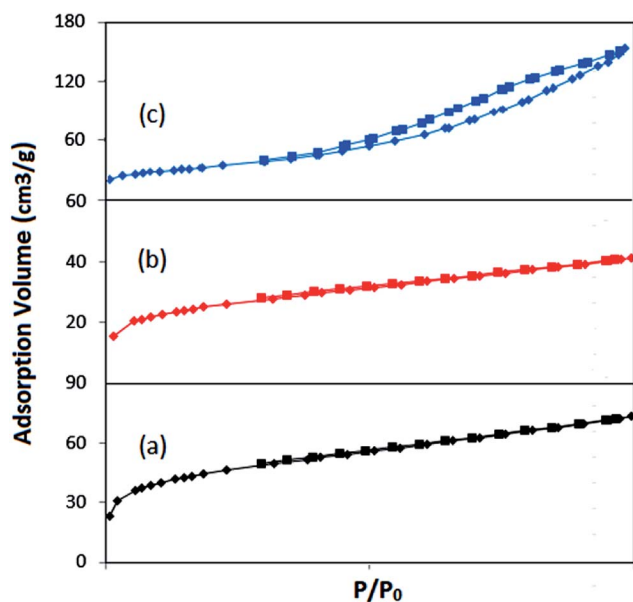


Fig. 5  $N_2$  adsorption–desorption spectra of (a)  $(NiFe_2O_4@Cu)SO_2(MMT)$ , (b)  $(NiFe_2O_4@Cu)(MMT-SO_3H)$  and (c)  $(NiFe_2O_4@Cu)(MMT)$ .

materials with the extreme of tiny pores.<sup>72</sup> It is noteworthy that after the immobilization of  $NiFe_2O_4@Cu$  MNPs, the BET surface area and total pore volume of all samples were substantially decreased *versus* to that of MMT-K10 (Table 3). This is attributed to blocking of some of pores in montmorillonite K10 by  $NiFe_2O_4@Cu$  MNPs.<sup>73</sup> Based on BDDT classification, the shape of isotherm in  $(NiFe_2O_4@Cu)(MMT)$  is adopted to isotherm type IV with a H3 hysteresis loop indicating micro- and mesoporous materials with an average pore diameter of 8 nm. Table 3 shows that  $(NiFe_2O_4@Cu)SO_2(MMT)$  MNPs has a high surface area in comparison to other samples. This increasing may be due to modification of  $Na^+$ -MMT with  $ClSO_3H$  leading to raise of specific surface area and total pore volume.<sup>74</sup> However, the immobilization of  $NiFe_2O_4@Cu$  MNPs over sulfonated sodium montmorillonite ( $Na^+$ -MMT- $SO_3H$ ) reduces the surface area and total pore volume.

**3.2.4. FT-IR analysis.** Fig. 6 shows FT-IR spectra of  $Na^+$ -MMT, MMT- $SO_3H$ ,  $NiFe_2O_4@Cu$  and  $(NiFe_2O_4@Cu)SO_2(MMT)$  clay composite systems. In the case of  $Na^+$ -MMT (Fig. 6a), the absorption band at  $3620\text{ cm}^{-1}$  is attributed to the vibration of bonded-OH to Al or Mg ions in  $Na^+$ -MMT. As well, the bands at  $3433\text{ cm}^{-1}$  and  $1635\text{ cm}^{-1}$  are also showing OH stretching and deforming vibrations of adsorbed water in interlayers of

montmorillonite. The bands at  $1054\text{ cm}^{-1}$  and  $800\text{ cm}^{-1}$  can be assigned to stretching vibration of Si–O. Moreover, the bands at  $522\text{ cm}^{-1}$  and  $464\text{ cm}^{-1}$  are also attributed to the vibration of Al–O and Si–O bonds, respectively.<sup>75–77</sup> FT-IR spectrum of MMT- $SO_3H$  (Fig. 6b) shows that the absorption bands of OH groups in montmorillonite and  $SO_3H$  were overlapped and produced a wide absorption signal at  $3000\text{--}3333\text{ cm}^{-1}$ . Moreover, the broad band at  $1048\text{ cm}^{-1}$  is also attributed to overlap vibrating bonds of S–O and Si–O in the composite system. In the case of  $(NiFe_2O_4@Cu)SO_2(MMT)$  (Fig. 6d), it is seen that through the immobilization of  $(NiFe_2O_4@Cu)$  moiety on sulfonated montmorillonite, the intensity of absorption band at  $3400\text{ cm}^{-1}$  was downed. This is exactly demonstrated the interaction of hydroxyl groups of MMT- $SO_3H$  and  $NiFe_2O_4@Cu$  moieties.

**3.2.5. VSM analysis.** Magnetic property of  $NiFe_2O_4$ ,  $NiFe_2O_4@Cu$ ,  $(NiFe_2O_4@Cu)SO_2(MMT)$ ,  $(NiFe_2O_4@Cu)(MMT-SO_3H)$  and  $(NiFe_2O_4@Cu)(MMT)$  was investigated using vibrating sample magnetometer analysis in an applied magnetic field up to 20 kOe (Fig. 7). All samples exhibited a characteristic magnetic hysteresis loop of soft magnetic materials.<sup>78</sup> The saturation magnetization ( $M_s$ ) value of  $NiFe_2O_4$  (curve a) and  $NiFe_2O_4@Cu$  (curve b) was found to be  $37.718\text{ emu g}^{-1}$  and  $34.584\text{ emu g}^{-1}$ , respectively. This shows that magnetic property of  $NiFe_2O_4$  and  $NiFe_2O_4@Cu$  MNPs is greater than  $(NiFe_2O_4@Cu)SO_2(MMT)$  (curve c),  $(NiFe_2O_4@Cu)(MMT)$  (curve d), and  $(NiFe_2O_4@Cu)(MMT-SO_3H)$  (curve e). It is demonstrating that through conjunction of the magnetic part of  $NiFe_2O_4$  with montmorillonite moiety,  $M_s$  value of the prepared clay composite system is impressively decreased. In this context, the saturation magnetization ( $M_s$ ) value is exactly rationalized to mass ratio of  $NiFe_2O_4$  in the nanocomposite systems. As well, the  $M_s$  value of  $NiFe_2O_4@Cu$  (curve b) is less than  $NiFe_2O_4$  (curve a) indicating contribution of diamagnetic copper nanoparticles. As shown in Fig. 7f, the magnetic nanoparticles of  $(NiFe_2O_4@Cu)SO_2(MMT)$ , because of high magnetization, showed an excellent response to the applied external magnetic field (2 min).

### 3.3. Synthesis of coumarin-based 1,4-dihydropyridines catalyzed by $(NiFe_2O_4@Cu)SO_2(MMT)$ MNPs

At the next attempt, catalytic activity of the prepared  $(NiFe_2O_4@Cu)SO_2(MMT)$  MNPs was studied towards Hantzsch synthesis of coumarin-based 1,4-dihydropyridines by one-pot and three-component condensation reaction of 4-hydroxycoumarin, aromatic aldehydes and ammonia. This

Table 3 Surface properties of the prepared clay nanocomposite systems<sup>a,b</sup>

Samples	$S_{BET}$ ( $m^2\text{ g}^{-1}$ )	$V_m$ ( $cm^3\text{ g}^{-1}$ )	Average pore diameter (nm)	$V_p$ ( $cm^3\text{ g}^{-1}$ )	Total pore volume ( $cm^3\text{ g}^{-1}$ )
MMT-K10	250.11	51.835	6.427	0.4016	0.4298
$(NiFe_2O_4@Cu)SO_2(MMT)$	128.19	29.45	3.52	0.0673	0.113
$(NiFe_2O_4@Cu)(MMT)$	119.52	27.46	7.92	0.232	0.236
$(NiFe_2O_4@Cu)(MMT-SO_3H)$	72.118	16.56	3.53	0.0381	0.0638
$NiFe_2O_4@Cu$	14.84	3.41	34.74	0.128	0.129

<sup>a</sup>  $S_{BET}$ : Brunauer–Emmett–Teller surface area. <sup>b</sup>  $V_p$ : BJH desorption cumulative volume of pores.



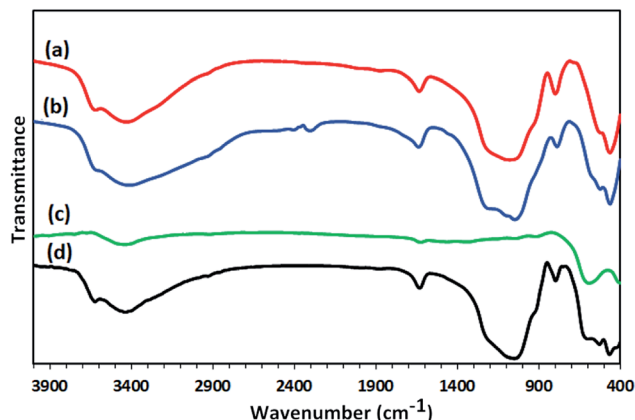


Fig. 6 FT-IR spectrum of (a) Na<sup>+</sup>-MMT, (b) MMT-SO<sub>3</sub>H, (c) NiFe<sub>2</sub>O<sub>4</sub>@Cu and (d) (NiFe<sub>2</sub>O<sub>4</sub>@Cu)SO<sub>2</sub>(MMT) NPs.

investigation was primarily carried out by optimizing the progress of the reaction of 4-hydroxycoumarin (2 mmol), 4-chlorobenzaldehyde (1 mmol) and ammonia (2 mmol) in the presence of (NiFe<sub>2</sub>O<sub>4</sub>@Cu)SO<sub>2</sub>(MMT) MNPs at different reaction conditions including the change of reaction-solvent, amount of catalyst and the source of nitrogen transferring agent. The illustrated results in Table 4 show that in the absence of the magnetic clay nanocatalyst, the condensation reaction did not any take place even at the prolonged reaction times (entries 1 and 2). However, the influence of (NiFe<sub>2</sub>O<sub>4</sub>@Cu)SO<sub>2</sub>(MMT) MNPs on the rate of model reaction is noteworthy. Entries 3–15 exhibited that by adding a small amount of NFCSM to the reaction mixture, the rate of condensation reaction was dramatically increased. The investigation for the influence of solvents such as H<sub>2</sub>O, H<sub>2</sub>O–EtOH, EtOH, EtOAc, CH<sub>3</sub>CN and

DMF or solvent-free conditions resulted that H<sub>2</sub>O exhibited a perfect rate enhancement. Therefore, H<sub>2</sub>O was selected as a solvent of choice. As well, changing the amount of nanocatalyst and temperature of the reaction revealed that using 10 mg of the nanocatalyst per 1 mmol of 4-chlorobenzaldehyde at 60 °C is the requirements to achieve the perfect efficiency. In addition, examining NH<sub>3</sub>, NH<sub>4</sub>OAc and NH<sub>4</sub>Cl as the sources of nitrogen represented that ammonia has the best ability to progress of the title reaction. Therefore, the condition mentioned in entry 12 (Table 4) was selected as the optimum reaction conditions (Scheme 2).

Next, the influence and catalytic activity of (NiFe<sub>2</sub>O<sub>4</sub>@Cu)SO<sub>2</sub>(MMT) MNPs was highlighted by comparing the yield and rate enhancement in condensation reaction of 4-hydroxycoumarin, 4-chlorobenzaldehyde and ammonia in the presence of Cu<sup>0</sup>, NiFe<sub>2</sub>O<sub>4</sub>, NiFe<sub>2</sub>O<sub>4</sub>@Cu, (NiFe<sub>2</sub>O<sub>4</sub>@Cu)(MMT) and (NiFe<sub>2</sub>O<sub>4</sub>@Cu)(MMT-SO<sub>3</sub>H) NPs at the optimized reaction conditions. The results of this investigation are summarized in Table 5. The obtained results exhibited that the clay containing sulfonyl-bridge represents a perfect catalytic activity as well as high yield of the product (Table 5, entry 4). Other modified clay composites, Cu<sup>0</sup> and NiFe<sub>2</sub>O<sub>4</sub> NPs encountered with low or unsatisfactory yield of 1,4-DHP at the same or prolonged reaction times.

Generality and usefulness of (NiFe<sub>2</sub>O<sub>4</sub>@Cu)SO<sub>2</sub>(MMT) MNPs towards Hantzsch synthesis of coumarin-based 1,4-DHPs was further studied by examining the condensation reaction of structurally diverse aromatic aldehydes, 4-hydroxycoumarin and ammonia in the presence of NFCSM at the optimized reaction conditions. The results of this investigation are illustrated in Table 6. The table shows that all reactions were carried

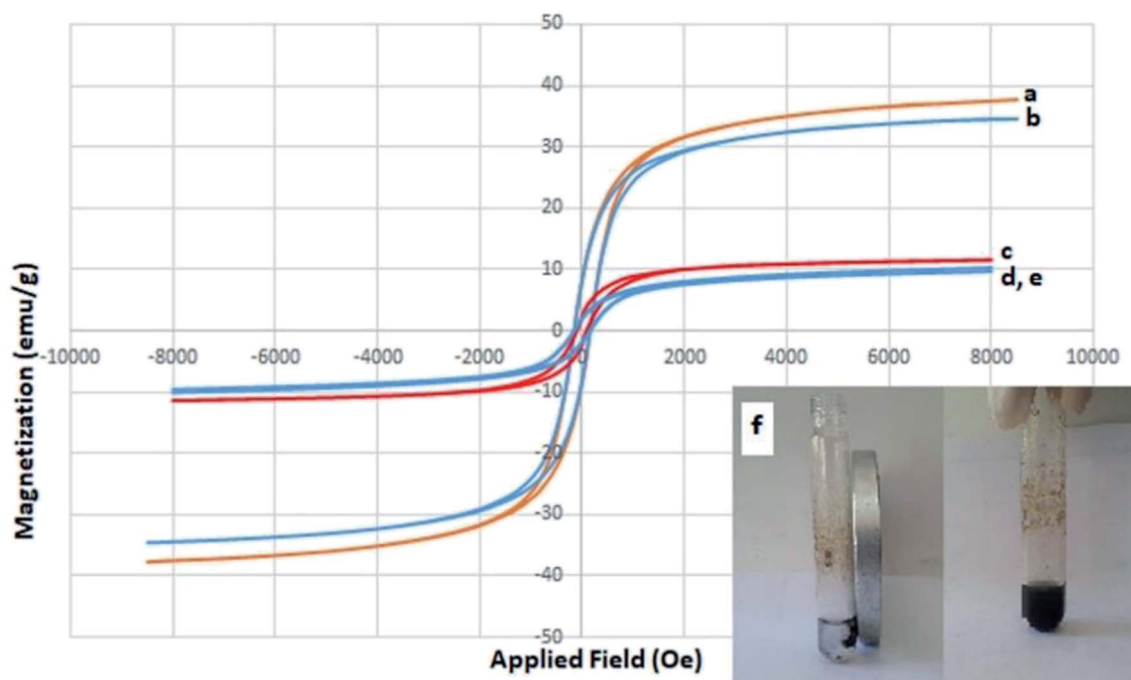
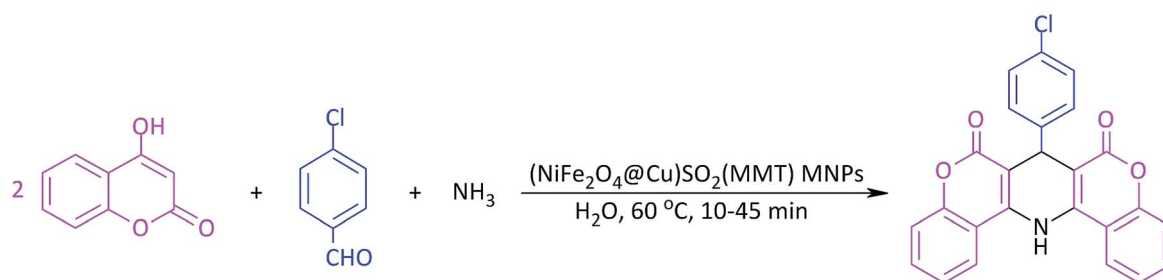


Fig. 7 Magnetization curves of (a) NiFe<sub>2</sub>O<sub>4</sub>, (b) NiFe<sub>2</sub>O<sub>4</sub>@Cu, (c) (NiFe<sub>2</sub>O<sub>4</sub>@Cu)SO<sub>2</sub>(MMT), (d) (NiFe<sub>2</sub>O<sub>4</sub>@Cu)(MMT-SO<sub>3</sub>H), (e) (NiFe<sub>2</sub>O<sub>4</sub>@Cu)(MMT) and (f) magnetic response of (NiFe<sub>2</sub>O<sub>4</sub>@Cu)SO<sub>2</sub>(MMT) MNPs.

**Table 4** Optimization experiments for condensation reaction of 4-chlorobenzaldehyde, 4-hydroxycoumarin and ammonia in the presence of (NiFe<sub>2</sub>O<sub>4</sub>@Cu)SO<sub>2</sub>(MMT) MNPs

Entry	(NiFe <sub>2</sub> O <sub>4</sub> @Cu)SO <sub>2</sub> (MMT) (mg)	Solvent (2 mL)	Temp (°C)	Amine	Time (min)	Yield (%)
1	—	EtOH	60	NH <sub>3</sub>	24 h	5
2	—	H <sub>2</sub> O	60	NH <sub>3</sub>	24 h	5
3	20	EtOH	60	NH <sub>3</sub>	45	60
4	20	H <sub>2</sub> O	60	NH <sub>3</sub>	20	98
5	20	EtOH–H <sub>2</sub> O (1 : 1)	60	NH <sub>3</sub>	30	90
6	20	EtOAc	60	NH <sub>3</sub>	200	45
7	20	CH <sub>3</sub> CN	60	NH <sub>3</sub>	200	50
8	20	DMF	60	NH <sub>3</sub>	120	50
9	20	Solvent-free	60	NH <sub>3</sub>	60	50
10	20	Solvent-free	Microwave	NH <sub>3</sub>	30	60
11	20	H <sub>2</sub> O	25	NH <sub>3</sub>	120	60
12	10	H <sub>2</sub> O	60	NH <sub>3</sub>	20	98
13	5	H <sub>2</sub> O	60	NH <sub>3</sub>	20	60
14	10	H <sub>2</sub> O	60	NH <sub>4</sub> OAc	50	40
15	10	H <sub>2</sub> O	60	NH <sub>4</sub> Cl	50	45

**Scheme 2** Hantzsch synthesis of coumarin-based 1,4-DHP (**4c**) catalyzed by (NiFe<sub>2</sub>O<sub>4</sub>@Cu)SO<sub>2</sub>(MMT) MNPs.**Table 5** Comparing the catalytic activity of (NiFe<sub>2</sub>O<sub>4</sub>@Cu)SO<sub>2</sub>(MMT) with other potentially active species in synthesis of 1,4-DHP (**4c**)<sup>a</sup>

Entry	Catalyst <sup>a</sup>	Time (min)	Yield <sup>b</sup> (%)
1	Cu <sup>0</sup> NPs	120	60
2	NiFe <sub>2</sub> O <sub>4</sub>	120	50
3	NiFe <sub>2</sub> O <sub>4</sub> @Cu	120	75
4	(NiFe <sub>2</sub> O <sub>4</sub> @Cu)SO <sub>2</sub> (MMT)	20	98
5	(NiFe <sub>2</sub> O <sub>4</sub> @Cu)(MMT)	20	80
6	(NiFe <sub>2</sub> O <sub>4</sub> @Cu)(MMT-SO <sub>3</sub> H)	20	85

<sup>a</sup> All reactions were carried out in H<sub>2</sub>O (2 mL) under oil bath (60 °C) conditions using 10 mg of nanocatalyst. <sup>b</sup> Isolated yield.

out successfully within 10–45 min to afford 1,4-DHPs in excellent yields. It is notable that the influence of substituents (aromatic rings) on the rate of reaction is noteworthy. Electron-withdrawing groups prolonged the reaction times and in contrast, electron-releasing groups enhance the rate of condensation reactions.

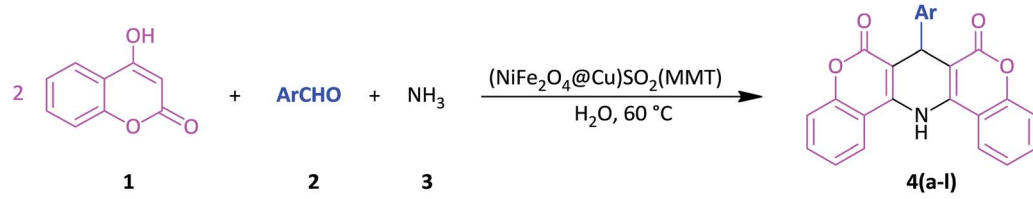
Although the exact mechanism of this synthetic protocol is not clear, however, a depicted mechanism (Scheme 3) shows a pathway for influence of the magnetic clay nanocatalyst on the formation of 1,4-DHPs. The scheme represents that through the activation of carbonyl group with the clay nanocomposite, the

Knoevenagel condensation of aldehyde and 4-hydroxycoumarin is taken place to afford intermediate **I**. By the reaction of intermediate **I** with ammonia, the imine intermediates **II** is produced. Activation of intermediate **II** with the clay nanocomposite followed by the reaction with the second molecule of 4-hydroxycoumarin affords the Michael adducts **III**. At the next, the imine intermediate **III** is tautomerized to produce enamine **IV**. Finally, nucleophilic attack of amino group towards carbonyl function make a ring closing product as 1,4-DHP.

The usefulness and capability of (NiFe<sub>2</sub>O<sub>4</sub>@Cu)SO<sub>2</sub>(MMT) MNPs in one-pot synthesis of coumarin-based 1,4-DHP (**4c**, derived by the reaction of 4-hydroxycoumarin, 4-chlorobenzaldehyde and ammonia) was also highlighted by comparing of the obtained result for NFCSM with the previously reported protocols (Table 7). A case study shows that in terms of reaction time, reusability of the promoter and yield of the product, the present work exhibits a more or comparable efficiency than the previous systems.

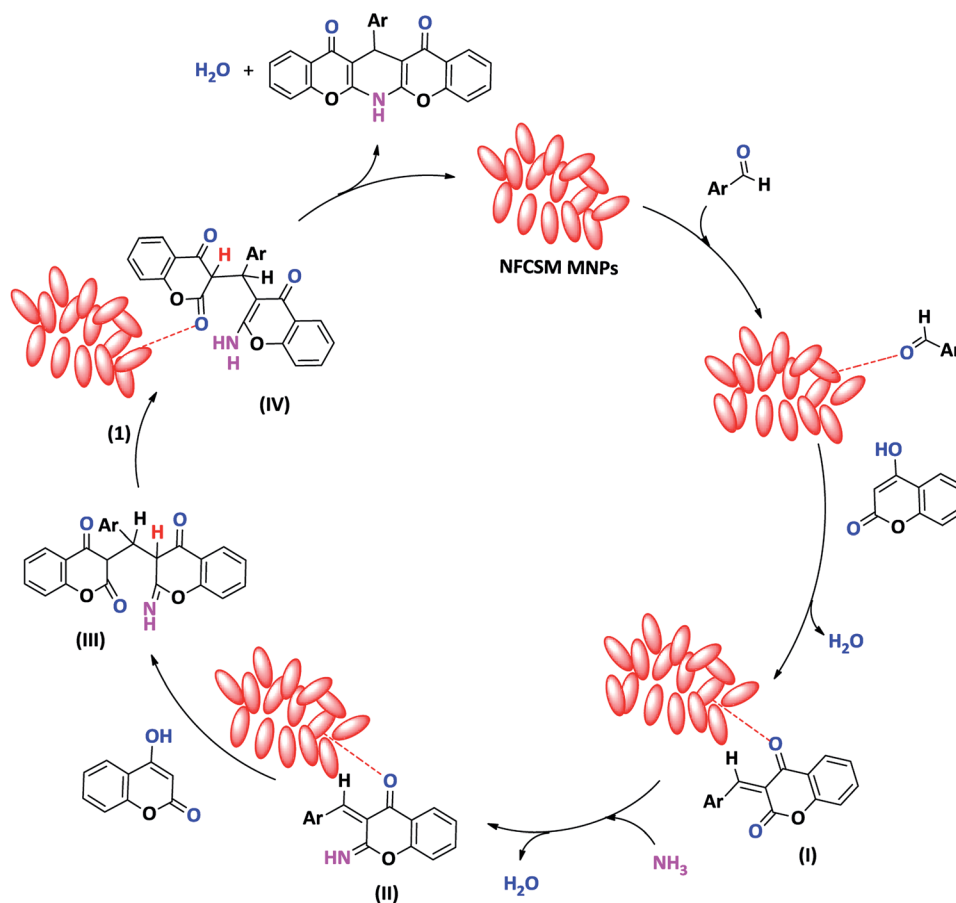
### 3.4. Recycling (NiFe<sub>2</sub>O<sub>4</sub>@Cu)SO<sub>2</sub>(MMT) MNPs

In order to examine the green and economic aspects of (NiFe<sub>2</sub>O<sub>4</sub>@Cu)SO<sub>2</sub>(MMT) MNPs as well the stability of (NiFe<sub>2</sub>O<sub>4</sub>@Cu) moiety on the surface of sulfonated montmorillonite, we also investigated reusability of the clay nanocomposite

Table 6 One-pot synthesis of coumarin-based 1,4-DHPs catalyzed by (NiFe<sub>2</sub>O<sub>4</sub>@Cu)SO<sub>2</sub>(MMT) MNPs<sup>a</sup>


Entry	Ar-	Product	(NiFe <sub>2</sub> O <sub>4</sub> @Cu)SO <sub>2</sub> (MMT) (mg)	Time (min)	Yield <sup>b</sup> (%)	Mp (°C)
1	C <sub>6</sub> H <sub>5</sub>	<b>4a</b>	10	20	95	185–187
2	2-ClC <sub>6</sub> H <sub>4</sub>	<b>4b</b>	10	25	90	215–217
3	4-ClC <sub>6</sub> H <sub>4</sub>	<b>4c</b>	10	20	98	220–222
4	3-OH, 4-MeOC <sub>6</sub> H <sub>3</sub>	<b>4d</b>	10	10	85	208–210
5	4-OH, 3-MeOC <sub>6</sub> H <sub>3</sub>	<b>4e</b>	10	10	90	210–214
6	3-MeOC <sub>6</sub> H <sub>4</sub>	<b>4f</b>	10	15	90	179–182
7	2-MeOC <sub>6</sub> H <sub>4</sub>	<b>4g</b>	10	10	85	196–198
8	4-MeC <sub>6</sub> H <sub>4</sub>	<b>4h</b>	10	15	90	190–192
9	4-OHC <sub>6</sub> H <sub>4</sub>	<b>4i</b>	10	20	85	172–174
10	4-O <sub>2</sub> NC <sub>6</sub> H <sub>4</sub>	<b>4j</b>	10	45	80	210–212
11	3-O <sub>2</sub> NC <sub>6</sub> H <sub>4</sub>	<b>4k</b>	10	30	75	208–211
12	3-O <sub>2</sub> N, 4-ClC <sub>6</sub> H <sub>3</sub>	<b>4l</b>	10	40	80	202–205

<sup>a</sup> All reactions were carried out in H<sub>2</sub>O (2 mL) at 60 °C. <sup>b</sup> Isolated yield.



Scheme 3 A proposed mechanism for NFCSM-catalyzed synthesis of coumarin-based 1,4-DHPs.

Table 7 Synthesis of coumarin-based 1,4-DHP (**4c**) by (NiFe<sub>2</sub>O<sub>4</sub>@Cu)SO<sub>2</sub>(MMT) and other reported systems<sup>a</sup>

Entry	Catalyst	Time (min)	Yield (%)	Condition	Reusability	Ref.
1	(NiFe <sub>2</sub> O <sub>4</sub> @Cu)SO <sub>2</sub> (MMT)	20	98	H <sub>2</sub> O (60 °C)	6	<sup>b</sup>
2	Fe <sub>3</sub> O <sub>4</sub> @SiO <sub>2</sub>	20	88	H <sub>2</sub> O (reflux)	4	59
3	Guanidinium-sulfonic acid	120	86	H <sub>2</sub> O (reflux)	4	60
4	Silica gel	25	65	Microwave	—	61
5	Acidic alumina	14	75	Microwave	—	61
6	Lactic acid	150	79	Ethyl-L-lactate (100 °C)	—	62

<sup>a</sup> 1,4-DHP (**4c**) was obtained by the reaction of 4-hydroxycoumarin (2 mmol), 4-chlorobenzaldehyde (1 mmol) and NH<sub>3</sub>, NH<sub>4</sub>OAc or NH<sub>4</sub>Cl (2 mmol).

<sup>b</sup> Present work.

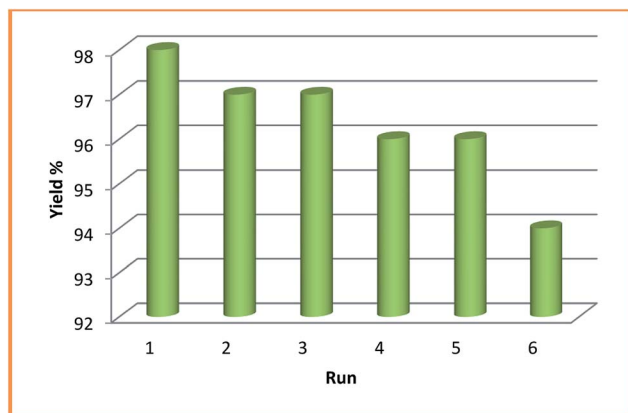


Fig. 8 Reusability of (NiFe<sub>2</sub>O<sub>4</sub>@Cu)SO<sub>2</sub>(MMT) MNPs.

system towards three-component condensation reaction of 4-hydroxycoumarin, 4-chlorobenzaldehyde and ammonia at the optimized reaction conditions. To do this, when the model reaction was completed, the clay nanocomposite was magnetically separated and washed with EtOH to remove any contaminants. After drying in an oven at 60 °C for 2 h, the model reaction was again charged with the fresh 4-hydroxycoumarin, 4-chlorobenzaldehyde and ammonia and the recycled clay nanocatalyst. Fig. 8 shows that the clay nanocatalyst, (NiFe<sub>2</sub>O<sub>4</sub>@Cu)SO<sub>2</sub>(MMT), can be reused for 6 consecutive cycles without the significant loss of its catalytic activity.

## 4. Conclusions

In this study, a new class of magnetic clay composite systems was synthesized. The clay nanocatalyst was prepared through the immobilization of NiFe<sub>2</sub>O<sub>4</sub>@Cu MNPs on the surface of sulfonated montmorillonite to afford (NiFe<sub>2</sub>O<sub>4</sub>@Cu)SO<sub>2</sub>(MMT) system. The magnetic NFCSM was then characterized using SEM, EDX, XRD, FTIR, BET and VSM analyses. Catalytic activity of the clay nanocatalyst was investigated towards Hantzsch synthesis of coumarin-based 1,4-dihydropyridines by one-pot and three-component condensation reaction of 4-hydroxycoumarin, aromatic aldehydes and ammonia in water as a green and economic solvent. All reactions were carried out within 10–45 min to afford 1,4-DHPs in excellent yields. Representing a new magnetic clay-based nanocatalyst, short

reaction times, low catalyst loading, high yield of the products, excellent reusability of the nanocatalyst as well as using water as a green solvent are the advantages which make this protocol a prominent choice for synthesis of coumarin-based 1,4-DHPs.

## Conflicts of interest

The authors declare no conflicts of interest.

## Acknowledgements

The authors gratefully acknowledge the financial support of this work by the research council of Urmia University.

## References

- 1 P. W. Davies, *Annu. Rep. Prog. Chem., Sect. B: Org. Chem.*, 2009, **105**, 93–112.
- 2 J. A. Gladysz, *Chem. Rev.*, 2002, **102**, 3215–3216.
- 3 C. S. Gill, B. A. Price and C. W. Jones, *J. Catal.*, 2007, **251**, 145–152.
- 4 J. A. Melero, R. van Grieken and G. Morales, *Chem. Rev.*, 2006, **106**, 3790–3812.
- 5 M. Sousa, E. Hasmonay, J. Depeyrot, F. Tourinho, J.-C. Bacri, E. Dubois, R. Perzynski and Y. L. Raikher, *J. Magn. Magn. Mater.*, 2002, **242**, 572–574.
- 6 M. H. Sousa, F. A. Tourinho, J. Depeyrot, G. J. da Silva and M. C. F. Lara, *J. Phys. Chem. B*, 2001, **105**, 1168–1175.
- 7 K. Sreekumar and S. Sugunan, *J. Mol. Catal. A: Chem.*, 2002, **185**, 259–268.
- 8 L. Luo, Q. Li, Y. Xu, Y. Ding, X. Wang, D. Deng and Y. Xu, *Sens. Actuators, B*, 2010, **145**, 293–298.
- 9 L. Yang, Y. Xie, H. Zhao, X. Wu and Y. Wang, *Solid-State Electron.*, 2005, **49**, 1029–1033.
- 10 A. Akther Hossain, M. Seki, T. Kawai and H. Tabata, *J. Appl. Phys.*, 2004, **96**, 1273–1275.
- 11 M. Salavati-Niasari, F. Davar and T. Mahmoudi, *Polyhedron*, 2009, **28**, 1455–1458.
- 12 V. Polshettiwar, R. Luque, A. Fihri, H. Zhu, M. Bouhrara and J.-M. Basset, *Chem. Rev.*, 2011, **111**, 3036–3075.
- 13 M. Zhang, Q. Zhang, T. Itoh and M. Abe, *IEEE Trans. Magn.*, 1994, **30**, 4692–4694.

- 14 I. J. Bruce, J. Taylor, M. Todd, M. J. Davies, E. Borioni, C. Sangregorio and T. Sen, *J. Magn. Magn. Mater.*, 2004, **284**, 145–160.
- 15 B. J. Borah, D. Dutta, P. P. Saikia, N. C. Barua and D. Kumar Dutta, *Green Chem.*, 2011, **13**, 3453–3460.
- 16 P. P. Sarmah and D. Kumar Dutta, *Green Chem.*, 2012, **14**, 1086–1093.
- 17 M. Tamura and H. Fujihara, *J. Am. Chem. Soc.*, 2003, **125**, 15742–15743.
- 18 V. K. Sharma, R. A. Yngard and Y. Lin, *Adv. Colloid Interface Sci.*, 2009, **145**, 83–96.
- 19 N. Mahata, A. Cunha, J. Órfão and J. Figueiredo, *Catal. Commun.*, 2009, **10**, 1203–1206.
- 20 M. Arruebo, R. Fernández-Pacheco, S. Irusta, J. Arbiol, M. R. Ibarra and J. Santamaría, *Nanotechnology*, 2006, **17**, 4057.
- 21 R. F. Ziolo, E. P. Giannelis, B. A. Weinstein, M. P. O'Horo, B. N. Ganguly, V. Mehrotra, M. W. Russell and D. R. Huffman, *Science*, 1992, **257**, 219–223.
- 22 A. Novakova, V. Y. Lanchinskaya, A. Volkov, T. Gendler, T. Y. Kiseleva, M. Moskvina and S. Zezin, *J. Magn. Magn. Mater.*, 2003, **258**, 354–357.
- 23 B. S. Kumar, A. Dhakshinamoorthy and K. Pitchumani, *Catal. Sci. Technol.*, 2014, **4**, 2378–2396.
- 24 O. S. Ahmed and D. Kumar Dutta, *Langmuir*, 2003, **19**, 5540–5541.
- 25 B. J. Borah, D. Dutta and D. Kumar Dutta, *Appl. Clay Sci.*, 2010, **49**, 317–323.
- 26 S. Zulfiqar, A. Kausar, M. Rizwan and M. I. Sarwar, *Appl. Surf. Sci.*, 2008, **255**, 2080–2086.
- 27 Z. Xu, F. Lv, Y. Zhang and L. Fu, *Chem. Eng. J.*, 2013, **215**, 755–762.
- 28 C. Galindo-Gonzalez, J. De Vicente, M. Ramos-Tejada, M. Lopez-Lopez, F. Gonzalez-Caballero and J. Duran, *Langmuir*, 2005, **21**, 4410–4419.
- 29 K. Kalantari, M. B. Ahmad, K. Shameli, M. Z. B. Hussein, R. Khandanlou and H. Khanehzaei, *J. Nanomater.*, 2014, **2014**, 181.
- 30 A. Bourlinos, M. Karakassides, A. Simopoulos and D. Petridis, *Chem. Mater.*, 2000, **12**, 2640–2645.
- 31 V. D. Cao, P. P. Nguyen, V. Q. Khuong, C. K. Nguyen, X. C. Nguyen, C. H. Dang and N. Q. Tran, *Bull. Korean Chem. Soc.*, 2014, **35**, 2645–2648.
- 32 M. Bottagisio, A. B. Lovati, F. Galbusera, L. Drago and G. Banfi, *Materials*, 2019, **12**, 314.
- 33 K. Bramhanwade, S. Shende, S. Bonde, A. Gade and M. Rai, *Environ. Chem. Lett.*, 2016, **14**, 229–235.
- 34 M. Valodkar, S. Modi, A. Pal and S. Thakore, *Mater. Res. Bull.*, 2011, **46**, 384–389.
- 35 M. B. Gawande, A. Goswami, F.-X. Felpin, T. Asefa, X. Huang, R. Silva, X. Zou, R. Zboril and R. S. Varma, *Chem. Rev.*, 2016, **116**, 3722–3811.
- 36 B. Zeynizadeh, I. Mohammadzadeh, Z. Shokri and S. A. Hosseini, *J. Colloid Interface Sci.*, 2017, **500**, 285–293.
- 37 Z. Shokri and B. Zeynizadeh, *J. Iran. Chem. Soc.*, 2017, **14**, 2467–2474.
- 38 V. D. Kancheva, P. V. Boranova, J. T. Nechev and I. I. Manolov, *Biochimie*, 2010, **92**, 1138–1146.
- 39 J. C. Jung and O. S. Park, *Molecules*, 2009, **14**, 4790–4803.
- 40 N. Hamdi, M. C. Puerta and P. Valerga, *Eur. J. Med. Chem.*, 2008, **43**, 2541–2548.
- 41 K. A. Nolan, H. Zhao, P. F. Faulder, A. D. Frenkel, D. J. Timson, D. Siegel, D. Ross, T. R. Burke Jr, I. J. Stratford and A. R. Bryce, *J. Med. Chem.*, 2007, **5**, 6316–6325.
- 42 M. Choudhary, N. Fatima, K. M. Khan, S. Jalil, S. Iqbal and A. U. Rahman, *Bioorg. Med. Chem.*, 2006, **14**, 8066–8072.
- 43 I. Kostova, G. Momekov, M. Zaharieva and M. Karaivanova, *Eur. J. Med. Chem.*, 2005, **40**, 542–551.
- 44 K. M. Khan, S. Iqbal, M. A. Lodhi, G. M. Maharvi, Z. Ullah, M. I. Choudhary, A. U. Rahman and S. Perveen, *Bioorg. Med. Chem.*, 2004, **12**, 1963–1968.
- 45 N. O. Mahmoodi, F. Ghanbari Pirbasti and Z. Jalalifard, *J. Chin. Chem. Soc.*, 2018, **65**, 383–394.
- 46 K. Tabatabaeian, H. Heidari, A. Khorshidi, M. Mamaghani and N. O. Mahmoodi, *J. Serb. Chem. Soc.*, 2012, **77**, 407–413.
- 47 V. K. Sharma and S. K. Singh, *RSC Adv.*, 2017, **7**, 2682–2732.
- 48 M. George, L. Joseph and C. Joseph, *Pharma Innovation*, 2017, **6**, 165–170.
- 49 G. W. Zamponi, *Nat. Rev. Drug Discovery*, 2016, **15**, 19–34.
- 50 P. A. Datar and P. B. Auti, *J. Saudi Chem. Soc.*, 2016, **20**, 510–516.
- 51 S. A. Khedkar and P. B. Auti, *Mini-Rev. Med. Chem.*, 2014, **14**, 282–290.
- 52 R. S. Kumar, A. Idhayadulla, A. J. A. Nasser and J. Selvin, *J. Serb. Chem. Soc.*, 2011, **76**, 1–11.
- 53 R. S. Kumar, A. Idhayadulla, A. J. A. Nasser and K. Murali, *Indian J. Chem.*, 2011, **50B**, 1140–1144.
- 54 G. Swarnalatha, G. Prasanthi, N. Sirisha and C. Madhusudhana Chetty, *Int. J. ChemTech Res.*, 2011, **3**, 75–89.
- 55 C. Bladen, V. M. Gadotti, M. G. Gündüz, N. D. Berger, R. Şimşek, C. Şafak and G. W. Zamponi, *Pflügers Arch.*, 2014, **467**, 1237–1247.
- 56 N. Edraki, A. R. Mehdipour, M. Khoshneviszadeh and R. Miri, *Drug Discovery Today*, 2009, **14**, 1058–1066.
- 57 D. J. Triggle, *Curr. Pharm. Des.*, 2006, **12**, 443–457.
- 58 R. Peri, S. Padmanabhan, A. Rutledge, S. Singh and D. J. Triggle, *J. Med. Chem.*, 2000, **43**, 2906–2914.
- 59 B. Dam, S. Nandi and A. K. Pal, *Tetrahedron Lett.*, 2014, **55**, 5236–5240.
- 60 A. Shaabani, S. Shaabani, M. Seyyedhamzeh, M. H. Sangachin and F. Hajishaabanha, *Res. Chem. Intermed.*, 2016, **42**, 7247–7256.
- 61 M. Kidwai, S. Rastogi and R. Mohan, *Bull. Korean Chem. Soc.*, 2004, **25**, 119–121.
- 62 S. Paul and A. R. Das, *Tetrahedron Lett.*, 2012, **53**, 2206–2210.
- 63 B. Zeynizadeh and F. Sepehraddin, *J. Organomet. Chem.*, 2018, **856**, 70–77.
- 64 B. Zeynizadeh and F. Sepehraddin, *J. Iran. Chem. Soc.*, 2017, **14**, 2649–2657.
- 65 S. Karami, B. Zeynizadeh and Z. Shokri, *Cellulose*, 2018, **25**, 3295–3305.

- 66 D. Dutta, B. J. Borah, L. Saikia, M. G. Pathak, P. Sengupta and D. Kumar Dutta, *Appl. Clay Sci.*, 2011, **53**, 650–656.
- 67 F. Shirini, M. Mamaghani and S. V. Atghia, *Catal. Commun.*, 2011, **12**, 1088–1094.
- 68 G. B. B. Varadwaj, S. Rana and K. Parida, *Chem. Eng. J.*, 2013, **215**, 849–858.
- 69 G. B. B. Varadwaj, S. Rana, K. Parida and B. B. Nayak, *J. Mater. Chem. A*, 2014, **2**, 7526–7534.
- 70 M. Auta and B. Hameed, *J. Ind. Eng. Chem.*, 2013, **19**, 1153–1161.
- 71 M. Mekewi, A. Darwish, M. Amin, G. Eshaq and H. Bourazan, *Egypt. J. Pet.*, 2016, **25**, 269–279.
- 72 S. Brunauer, L. S. Deming, W. E. Deming and E. Teller, *J. Am. Chem. Soc.*, 1940, **62**, 1723–1732.
- 73 S. K. Bhorodwaj, M. G. Pathak and D. Kumar Dutta, *Catal. Lett.*, 2009, **133**, 185.
- 74 P. K. Saikia, P. P. Sarmah, B. J. Borah, L. Saikia, K. Saikia and D. Kumar Dutta, *Green Chem.*, 2016, **18**, 2843–2850.
- 75 B. Tyagi, C. D. Chudasama and R. V. Jasra, *Appl. Clay Sci.*, 2006, **31**, 16–28.
- 76 J. Madejova and P. Komadel, *Clays Clay Miner.*, 2001, **49**, 410–432.
- 77 K. Wang, L. Wang, J. Wu, L. Chen and C. He, *Langmuir*, 2005, **21**, 3613–3618.
- 78 K. R. Reddy, W. Park, B. C. Sin, J. Noh and Y. Lee, *J. Colloid Interface Sci.*, 2009, **335**, 34–39.